ARTICLE OPEN

Check for updates

Demonstration of the effect of stirring on nucleation from experiments on the International Space Station using the ISS-EML facility

A. K. Gangopadhyay [1][✉], M. E. Sellers[1], G. P. Bracker [2], D. Holland-Moritz[3], D. C. Van Hoesen[1], S. Koch[4], P. K. Galenko[4], A. K. Pauls[2], R. W. Hyers[2] and K. F. Kelton [1]

The effect of fluid flow on crystal nucleation in supercooled liquids is not well understood. The variable density and temperature gradients in the liquid make it difficult to study this under terrestrial gravity conditions. Nucleation experiments were therefore made in a microgravity environment using the Electromagnetic Levitation Facility on the International Space Station on a bulk glass-forming $Zr_{57}Cu_{15.4}Ni_{12.6}Al_{10}Nb_5$ (Vit106), as well as $Cu_{50}Zr_{50}$ and the quasicrystal-forming $Ti_{39.5}Zr_{39.5}Ni_{21}$ liquids. The maximum supercooling temperatures for each alloy were measured as a function of controlled stirring by applying various combinations of radio-frequency positioner and heater voltages to the water-cooled copper coils. The flow patterns were simulated from the known parameters for the coil and the levitated samples. The maximum nucleation temperatures increased systematically with increased fluid flow in the liquids for Vit106, but stayed nearly unchanged for the other two. These results are consistent with the predictions from the Coupled-Flux model for nucleation.

npj Microgravity (2021)7:31 ; https://doi.org/10.1038/s41526-021-00161-9

INTRODUCTION

Crystal nucleation[1] and subsequent growth[2] in supercooled liquids (i.e., liquids at a temperature below the equilibrium melting temperature, T_l) are the two fundamental processes that determine the solidification microstructure[3]. Studies of these processes, then, occupy a central role in condensed matter physics, materials science, and biology. Both thermodynamic and kinetic factors influence nucleation and growth. In nucleation, spontaneous random processes in the liquid lead to the formation of dense, ordered, regions that are characteristic of the nucleating crystal. The growth of these ordered regions is stochastic, which may grow and shrink. Above a critical size it becomes thermodynamically favored for these aggregates to increase in size, eventually leading to their growth into crystalline solids. Homogeneous nucleation is controlled solely by the intrinsic properties of the liquid and nucleating phases and the amount of supercooling. In contrast, heterogeneous nucleation is catalyzed by foreign objects such as undissolved impurities or the container walls. The minimization of these catalytic sites is then crucial for the studies of homogeneous nucleation; containerless processing, using electrostatic (ESL)[4], electromagnetic (EML)[5], aerodynamic[6], and acoustic[7] levitation, allows such studies. While useful for oxide materials, aerodynamic and acoustic levitations are not recommended for metallic liquids since even the highest purity inert gases often contain impurities that catalyze nucleation.

Nucleation is known to be influenced by pressure[8], electric[9,10] and magnetic fields[11], and it has been shown to couple with other phase transitions, such as magnetic transition in a liquid[12,13]. The effect of forced convection on crystal growth has also been studied in a number of recent publications[14,15]. However, the effect of stirring (fluid flow) on nucleation in a liquid is not well established. A model was developed for cases where the

nucleating phase has a different chemical composition than the initial phase (the coupled-flux model[16]). In this case, the growth of the nuclei leads to a change in chemical composition near the cluster. This interacts with the long-range diffusion field, leading to a coupling of the stochastic processes of interfacial kinetics and diffusion. If the interfacial attachment/detachment rates are faster than the diffusion rate, the kinetics of nucleation can be significantly decreased. The coupled-flux model has been explored numerically[17] and has been applied successfully for the precipitation of oxygen in single crystal silicon[18]. For crystal nucleation from a quiescent liquid of a different chemical composition, the coupled fluxes should decrease the nucleation rate. If the liquid is stirred, however, the fluid flow should enhance solute transport and the nucleation rate should increase toward the expected steady-state nucleation rate. To our knowledge, a systematic study of the effect of stirring on nucleation of solids from supercooled liquids does not exist.

Here, we report the results of studies of the effect of stirring on nucleation in electromagnetically levitated metallic liquid drops under the microgravity environment of the International Space Station (ISS). Such controlled stirring experiments are not possible under terrestrial conditions because of the natural density and surface tension (Marangoni)[19] driven convection. Microgravity eliminates the first because of the absence of gravity-induced flows. Nearly uniform heating of the sample with a radio-frequency (rf) electromagnetic field in the EML minimizes the second. The EML facility on the ISS, ISS-EML[20], is capable of controlling the fluid flow by electromagnetic stirring. A brief description of the facility can be found in the "Methods" section. Three different alloys were chosen to investigate the effect of stirring on nucleation rates in supercooled liquids for different solidification motifs (polymorphic and multiphase). A $Ti_{39.5}Zr_{39.5}Ni_{21}$ alloy in which primary nucleation

[1]Department of Physics and the Institute of Materials Science and Engineering, Washington University in St. Louis, USASt. Louis, MO. [2]Department of Mechanical and Industrial Engineering, University of Massachusetts, Amherst, MA, USA. [3]Institut für Materialphysik im Weltraum, Deutsches Zentrum für Luft- und Raumfahrt (DLR), Köln, Germany. [4]Otto-Schott-Institut für Materialforschung, Friedrich Schiller Universität Jena, Jena, Germany. ✉email: anup@wuphys.wustl.edu
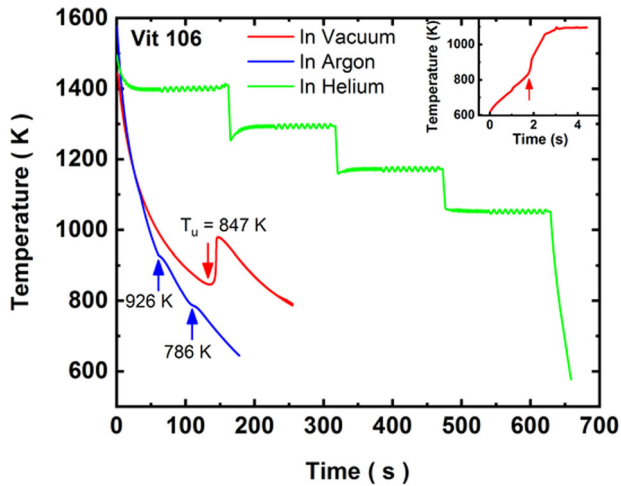
A.K. Gangopadhyay et al.

Fig. 1 Typical time–temperature plots during cooling of a Vit106 ($Zr_{57}Cu_{15.4}Ni_{12.6}Al_{10}Nb_5$) liquid under vacuum, Ar, and He atmospheres. Complete and partial crystallizations happened in vacuum and under Ar atmospheres. The arrows indicate the crystallization events. Crystallization was completely suppressed in He atmosphere due to a much faster cooling. The inset shows the recalescence rise in temperature when the glass transformed into crystals during the next heating cycle.

is to a quasicrystal of the same composition[21,22] was one choice. It was observed that, although metastable, the quasicrystal phase nucleates first from the supercooled liquid, followed by its decomposition into the stable Laves and solid-solution phases at higher temperatures as the liquid temperature increased due to the release of the heat of fusion. The other two were the bulk metallic glass-forming $Cu_{50}Zr_{50}$ and $Zr_{57}Cu_{15.4}Ni_{12.6}Al_{10}Nb_5$ (Vit106) alloys. The primary crystallizing phase from the $Cu_{50}Zr_{50}$ liquid is a cubic B2 phase of $CuZr$[23], which is consistent with the phase diagram[24]. In contrast, crystalline phases of Zr_2Ni, Zr_2Cu, $ZrCu$, Zr_3Al_2, and Zr_4Al_3, which also contain various amounts of other elements, crystallize from the glass of Vit106[25]. The results obtained clearly demonstrate that increased stirring increases the nucleation rate for the Vit106, which shifts the crystallization to higher temperatures; little or no effect of stirring was observed for the other two. The results are consistent with the expectations from the coupled-flux model. This is a new observation which is of considerable interest for a fundamental understanding of the nucleation mechanism in partitioning systems. These results could be also vitally important for the future processing of materials in space, which will be necessary for long-term space explorations, and ultimately for manufacturing under extra-terrestrial conditions on Mars and the Moon.

RESULTS

Nucleation studies of Vit106, $Cu_{50}Zr_{50}$, and $Ti_{39.5}Zr_{39.5}Ni_{21}$ liquids on the ISS

The experimental details are described in the "Methods" section of this paper and in refs. [20,26]. Independent control of the heating and positioning of a sample in the ISS-EML is one of the advantages compared to the ground-based EML facilities. Two different electronic circuits feed currents into a pair of identical Cu coils for sample positioning and heating. The rf-electromagnetic fields generated by these currents interact with the electrons in the solid/liquid generating eddy currents, which affect fluid flow[26]. Since these rf fields can be controlled by different combinations of heater and positioner voltages, stirring in liquids can be controlled systematically. Because of the stronger coupling of the heater to the sample, the heater voltage/current is more effective than the

positioner in increasing stirring in the liquid[20,26]. The samples were processed under vacuum (10^{-8} mbar) and in 350 mbar Ar and He atmospheres. Figure 1 shows typical time–temperature data for a 6.0 mm diameter Vit106 liquid sphere that was cooled under vacuum from 1440 K, and in a 350 mbar Ar and He atmospheres from 1550 K ($T_l = 1123K$) with a 2.5 V positioner voltage and the heater off. The sudden rise in temperature at 847 K under vacuum marks the nucleation and growth of the crystal phases from the liquid; the temperature rise is due to the release of heat of fusion during solidification. The onset of the recalescence (nucleation temperature, T_u) marks the limit of supercooling (276 K = 0.246T_l) for this particular thermal cycle. Note that the recalescence temperature does not rise to T_l since the sample cooled below the hypercooling limit (~230–250 K). The cooling rate near the onset temperature for recalescence was 1.3 K/s, which was not sufficient to prevent crystallization. However, the higher cooling rate of 2.2 K/s in the Ar atmosphere almost suppressed crystallization; only two small kinks near 926 and 786 K were observed. When processed in He atmosphere, a much faster cooling rate of 15 K/s was achieved around 850 K, which completely suppressed crystallization, as shown in Fig. 1. This thermal cycle was used for specific heat measurements by modulating the temperature at various hold temperatures. After the last modulation at 1050 K, the heater was turned off for rapid cooling. No crystallization event was observed. That this sample transformed into a glass was evident when it was heated in the next thermal cycle. A sudden rise in temperature due to a glass-crystal transformation was observed between 834 and 922 K, as shown in the inset of Fig. 1. This thermal event is similar to observations made in ground-based ESL studies when a glass was heated rapidly[27]. Unfortunately, subsequent processing of the sample in the He atmosphere caused contamination, possibly from trace amounts of oxygen in the gas, which prevented glass formation. Our ground-based studies[27] indicated that 500–600 ppm oxygen is enough to prevent bulk glass formation in this alloy. A similar observation of glass formation in a Vit105 ($Zr_{52.5}Cu_{17.9}Ni_{14.6}Al_{10}Ti_5$) alloy under microgravity was reported earlier[28]; this is then the second demonstration that a bulk metallic glass (6.0 mm diameter) can be manufactured in space. Although not unexpected, this result may be of importance for future space-based manufacturing of intricate machine parts using bulk metallic glasses.

When a 6.5 mm diameter $Cu_{50}Zr_{50}$ liquid sample was cooled in the ISS-EML using a small positioner voltage (3.9 V) and heater off under vacuum, the sample supercooled by 252 K (0.206T_l, $T_l =$ 1222 K), which is less than the value of 322 K observed in ground-based ESL studies of a much smaller sample (2.5 mm diameter)[29], most likely due to a faster cooling rate. In comparison, a 6.0 mm diameter $Ti_{39.5}Zr_{39.5}Ni_{21}$ liquid in the ISS-EML supercooled by 87 K (0.082T_l, $T_l = 1063$ K) for the metastable icosahedral phase under similar conditions because the structure of the icosahedral phase is similar to that of the liquid[21,30]. Note that if the transformation of the icosahedral phase into a mixture of stable Ti–Zr solid solution and Laves phase can be suppressed, it melts at 1063 K, compared to 1093 K for the phase mixture of the same composition[31]. A slightly higher supercooling of 110 K was possible in the ground-based ESL studies of this liquid[32]. These differences in supercoolability may be due to many factors, such as slower cooling rates (about 3 K/s near T_u compared to about 12 K/s in the ESL) for the larger samples used in space, larger sample volume, larger stirring due to eddy currents induced in the liquid by the EML, and/or small differences in sample purities. The question whether these are homogeneous or heterogeneous nucleation due to small amounts of impurities will be discussed later.

Since nucleation is a stochastic process, a distribution of nucleation temperatures for a large number of heating and cooling cycles is usually observed[33]. Typically, many hundreds of cycles are required to obtain statistically significant data for this distribution[29,32,34,35]. To obtain a statistically significant result for the effect of stirring, then, many thermal cycles for the same heater and

Table 1. Experimental data for Vit106 (Zr₅₇Cu₁₅.₄Ni₁₂.₆Al₁₀Nb₅).

Average nucleation temperature, T_u (K)	Supercooling (K)	Positioner voltage (V)	Heater voltage (V)	Fluid flow velocity at T_u (ms⁻¹)	Shear rate at T_u (s⁻¹)	Interfacial energy, σ (Jm⁻²)	A^* (m⁻³ s⁻¹)
853	270	2.5	Off	1.3×10^{-7}	3×10^{-4}	0.12	2.5×10^{35}
860	263	3.4	Off	1.9×10^{-7}	3.9×10^{-4}	0.12	6×10^{36}
872	251	4.3	Off	7.4×10^{-7}	0.0017	0.12	7×10^{38}
880	243	6.0	Off	2.2×10^{-6}	0.0035	0.12	7×10^{40}

Table 2. Experimental data for Cu₅₀Zr₅₀.

Average nucleation temperature, T_u (K)	Supercooling (K)	Positioner voltage (V)	Heater voltage (V)	Fluid flow velocity at T_u (ms⁻¹)	Shear rate at T_u (s⁻¹)	Interfacial energy, σ (Jm⁻²)	A^* (m⁻³ s⁻¹)
970	252	3.9	Off	2.5×10^{-4}	0.49	0.100	5×10^{33}
973	249	4.8	Off	3.5×10^{-4}	0.71	0.100	2×10^{34}

positioner voltages must be performed. However, processing in the ISS-EML is restricted by several considerations. To enhance the life of the facility, each sample is allotted a certain amount of mass loss due to evaporation, part of which deposits on the Cu coils. In addition to nucleation studies, thermophysical properties (viscosity, surface tension, and specific heat) and electrical properties of the liquids were also measured. This restricted the number of melting cycles from three to five for a particular setting of the heater and positioner voltages. Lower vapor depositions on the Cu coils in the He-gas atmosphere allowed more thermal cycles (ten to twenty) to be performed. However, the number of such cycles is also restricted because of dust generation under a gas atmosphere which must be limited to protect the health of the astronauts, in case the EML chamber is accidentally exposed to the atmosphere of the crew cabin. Another problem was that once the samples were melted in gas atmospheres, the nucleation temperature started rising and reached a saturation level after a few cycles. Some surface features were also observed in the video images during the cooling of the liquid drops, indicating oxide precipitation. Therefore, the data collected in vacuum are considered to be more representative of homogeneous nucleation than those in the gas atmospheres. For that reason, the data presented here are from vacuum processing only. The experiments were conducted over several nights on the ISS due to restrictions on the allotted times on a given day.

According to the classical nucleation theory[1], the homogeneous nucleation rate, I(T), at a temperature, T, is given by

$$I(T) = A^* \exp(-W^*/k_B T) \quad (1)$$

where

$$W^* = 16\pi\sigma^3/3\Delta G^2 \quad (2)$$

The prefactor, A^*, primarily contains kinetic parameters, such as the diffusion coefficient, the atomic jump distance, and the number of possible sites for nucleation; W^* contains the interfacial free energy, σ, and the driving free energy, ΔG. If the nucleation temperature, T_u, is determined from several cycles for a sample of volume V, cooled below the liquidus temperature, T_l, at a rate of Q, it follows a Poisson's distribution with a probability density for nucleation, ω(t), given by[33]

$$\omega(t) = \frac{I(T)V}{Q} \exp\left(-\int_{T_u}^{T_l} \frac{I(T)V}{Q} dT\right) \quad (3)$$

By fitting the experimentally measured distribution to Eq. (3), the relevant nucleation parameters A^*, W^*, and σ may be determined. According to the coupled-flux model[16], A^* is the more appropriate parameter for studying the effects of stirring since it contains a combination of the interfacial attachment kinetics and the diffusion coefficient in the liquid. Initially, melting/solidification cycles were

performed in vacuum under the most quiescent condition possible (minimum positioner voltage and heater off) and the parameters A^*, W^*, and σ were determined by fitting to Eq. (3). Thereafter, to investigate the effect of stirring, σ was kept constant and A^* was varied to give the best fit to the nucleation data obtained with increased stirring. In all cases, the driving free energy was estimated using the Turnbull approximation[36], $\Delta G = \Delta H_f \Delta T/T_l$, where ΔH_f is the heat of fusion and ΔT is the magnitude of supercooling.

The fluid flow velocities and shear rates corresponding to each positioner and heater voltage settings were simulated following procedures described in refs. [37,38] and in the "Methods" section. One example of the fluid flow velocities and shear rates, as shown in Supplementary Fig. 2, evolves with decreasing temperatures and shows a distribution; it is largest along the surface of the sample in a direction about 40⁰ from the equatorial plane due to the distribution of the rf field along the sample geometry. The parameters used for comparison with the nucleation data are the maximum fluid flow velocities and shear rates at the nucleation temperature.

Stirring effect on nucleation during processing in vacuum

Extensive studies of homogeneous nucleation using the ground-based ESL to measure many hundreds of solidification cycles for Cu₅₀Zr₅₀[29] and Ti₃₉.₅Zr₃₉.₅Ni₂₁[32] liquids were reported earlier. Similar studies could not be made for the Vit106 alloy since the smaller (~2.5 mm diameter) samples required for the ESL studies formed glasses upon cooling, bypassing crystal nucleation. Unfortunately, as mentioned earlier, such a large number of cycles to obtain statistically significant data for nucleation was not possible with the ISS-EML facility. This prevented a full quantitative analysis of the Poisson's distribution for T_u according to Eq. (3). However, since the cooling rates under different heater and positioner voltages were different, Eq. (3) could still be applied to incorporate those differences. Instead of reproducing the statistical distribution, the focus was to match the average T_u by adjusting A^* and W^*. The average nucleation temperatures, nucleation parameters derived from the ISS-EML data using Eq. (3), corresponding heater, and positioner voltages are listed in Tables 1–3 for Vit106 and Cu₅₀Zr₅₀ and Ti₃₉.₅Zr₃₉.₅Ni₂₁, respectively. Note that the heater off and heater at 0 V are two different conditions since about 19 A current still flows in the coils when the heater is on at 0 V. The calculated maximum fluid flow velocities and shear rates at the nucleation temperature, T_u, are also included.

The values for A^* and σ for Cu₅₀Zr₅₀ obtained from the ground-based ESL studies[29] were 2.5×10^{31} m⁻³ s⁻¹ and 0.113 Jm⁻², which are slightly different from the ISS-based EML studies under the most quiescent conditions (minimum positioner voltage and heater off), as presented in Table 2. The values of A^* and σ from the ESL studies

Table 3. Experimental data for $Ti_{39.5}Zr_{39.5}Ni_{21}$.

Average nucleation temperature, T_u (K)	Supercooling (K)	Positioner voltage (V)	Heater voltage (V)	Fluid flow velocity at T_u (ms^{-1})	Shear rate at T_u (s^{-1})	Interfacial energy, σ (Jm^{-2})	A^* (m^{-3} s^{-1})
976	87	3.9	Off	3.9×10^{-4}	0.87	0.052	2×10^{23}
974	89	5.7	Off	7.8×10^{-4}	1.7	0.052	3×10^{22}
975	88	4.0	0.0	1.7×10^{-3}	3.9	0.052	6×10^{21}

for $Ti_{39.5}Zr_{39.5}Ni_{21}$[32] were 2.7×10^{25} m^{-3} s^{-1} and 0.057 Jm^{-2}, respectively, which are again slightly different from those obtained from the nucleation studies on the ISS under vacuum (Table 3). Such differences may be due to different purities of the samples in the ISS than those used in the ground-based ESL studies. However, since the same starting materials and same preparation conditions were used for all alloys prepared for the ISS and ground-based studies, possibly some small amount of contamination in the ISS samples may have occurred during long-term storage, transportation (vibrations during rocket acceleration/deceleration rattle the sample in the sample holder), and/or processing on the ISS; fluid flows may also be different under the most quiescent conditions possible in the ground-based ESL and ISS-EML. It could be debated then whether the nucleation in these liquids is homogeneous or heterogeneous. A few aspects of the data, however, indicate that homogenous nucleation was achieved. The prefactor, A^*, in Vit106 reached a value of 7×10^{40} with high stirring, in agreement with that expected for homogeneous, interface-limited, nucleation[36]. The A^* value for $Cu_{50}Zr_{50}$ is also reasonably large, and might have increased further with larger levels of stirring. Interestingly, the value of A^* in the $Ti_{39.5}Zr_{39.5}Ni_{21}$ liquid is much smaller. This might indicate heterogeneous nucleation, but why it is so different from the other two liquids is puzzling since the same high-purity Zr was used to prepare all of the samples and the other elemental metals were of similar purity. Further, the fabrication method used to prepare the samples was the same and they were all prepared under the same conditions. There is another possible explanation. Synchrotron x-ray structural studies have suggested that regions of developing local icosahedral order in the supercooled liquid catalyze the nucleation of the i-phase[21]. These would then serve as preferential sites for nucleation, acting in the same way as heterogeneous nucleation and giving a smaller value of A^*, reflecting the smaller number nucleation sites in the liquid. At this time, it is not possible to definitively determine which mechanism is correct and will require further investigation in future studies.

DISCUSSION

Irrespective of whether the nucleation is homogeneous or heterogeneous, the ISS data represented in Tables 1–3 demonstrate that A^* increased by several orders of magnitude for the Vit106 alloy and remained nearly constant for the other two liquids with increasing stirring. Note that, according to the coupled-flux model[16], the effect of stirring on nucleation is expected to be observed both for homogeneous and heterogeneous nucleation. The fluid flow calculations were made using the experimental data for the liquid viscosity, which was measured using the ground-based ESL facility, are presented in the Supplementary section (Supplementary Fig. 1). A typical fluid flow velocity distribution in a $Ti_{39.5}Zr_{39.5}Ni_{21}$ liquid is also shown in Supplementary Fig. 2 for illustration. The errors in those estimates are about ±5%.

To demonstrate that the changes in the nucleation parameters are due to stirring, Fig. 2 shows the logarithm of the prefactor, A^* as a function of shear rates for processing in vacuum for the Vit106 liquid. Clearly, A^* increases with the maximum shear rate at the nucleation temperature in the liquid due to electromagnetic stirring. Although A^* correlates well with both the maximum fluid
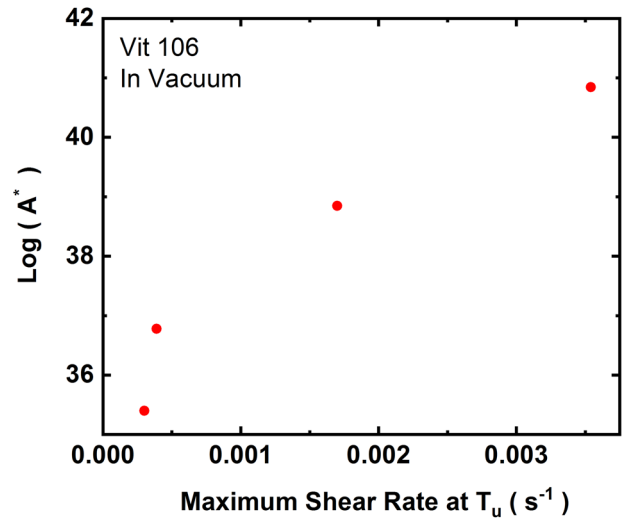

Fig. 2 The prefactor A^* for nucleation as a function of the maximum shear rate at the nucleation temperature (T_u) for processing in vacuum for liquid Vit106 ($Zr_{57}Cu_{15.4}Ni_{12.6}Al_{10}Nb_5$). The nucleation temperatures and the relevant parameters are presented in Table 1.

flow velocity and the maximum shear rate at T_u (see Tables 1–3), only the correlation with the shear rate is shown in Fig. 2 for clarity. The $Cu_{50}Zr_{50}$ liquid showed a small increase in A^* when the maximum fluid velocity increased from 2.5×10^{-4} to 3.5×10^{-4} ms^{-1} (Table 2). This small increase may not be statistically significant. Therefore, the results are consistent with expectations from the coupled-flux model, since the compositions of the liquid and the primary crystallizing phase are the same. However, more data are needed to make this conclusion statistically significant. Similar consideration applies to the changes in A^* with fluid flows for the $Ti_{39.5}Zr_{39.5}Ni_{21}$ liquid (Table 3). Note that the changes in A^* for the nearly similar values of T_u for this liquid are due to the slower cooling rates for the higher positioner voltages and heater on conditions.

In summary, two important new results emerge from this study. First, we have confirmed earlier studies[28], showing that bulk metallic glasses can be synthesized under microgravity. The second and most important observation is that the nucleation rate is significantly enhanced with increasing fluid flow when the composition changes during crystallization (Vit106), and little or no changes occur for polymorphic crystallization ($Cu_{50}Zr_{50}$ and $Ti_{39.5}Zr_{39.5}Ni_{21}$). For approximately an order of magnitude increase in the fluid flow velocities, the prefactor, A^*, increased by about five orders of magnitude for the Vit106 liquid (Table 1). This occurred even though the fluid flow velocities and the shear rates remained low throughout the range of experiments. For $Cu_{50}Zr_{50}$, A^* increased by about four times for about 40% increase in fluid flow velocity and shear rates. The correlation between A^* and fluid flow is less clear for the $Ti_{39.5}Zr_{39.5}Ni_{21}$ liquid; for three separate fluid flow conditions, A^* decreased by a factor of 33 for an increase in fluid flow by about a factor of 4. The data do clearly suggest

that for the $Cu_{50}Zr_{50}$ and $Ti_{39.5}Zr_{39.5}Ni_{21}$ liquids the effect of fluid flow on nucleation is much smaller than for the Vit106 liquid. According to the coupled-flux model[16], stirring should have a large effect on nucleation when compositional changes occur during solidification, since a concentration gradient is expected to develop in the vicinity of the nucleating cluster, as observed for Vit106. Smaller or no changes should be expected when little or no change in composition occurs during crystallization, as for the polymorphic crystallization for $Ti_{39.5}Zr_{39.5}Ni_{21}$ and $Cu_{50}Zr_{50}$ liquids. The data are then qualitatively consistent with the predictions of the coupled-flux model. A quantitative comparison will require more statistically significant data, obtained from hundreds of nucleation cycles. Future experiments on the ISS are planned for liquids that have lower vapor pressures so that nucleation data from a large number of thermal cycles can be obtained; the higher liquidus temperatures for these liquids will also facilitate higher levels of stirring.

METHODS

Sample preparation and nucleation measurements
Nearly spherical samples of $Ti_{39.5}Zr_{39.5}Ni_{21}$ (6.0 mm diameter), $Zr_{57}Cu_{15.4}Ni_{12.6}Al_{10}Nb_5$ (Vit106, 6.0 mm diameter), and $Cu_{50}Zr_{50}$ (6.5 mm diameter) were prepared on Earth by arc melting high-purity (>99.9 at.%) elements in the stoichiometric ratios in a $Ti_{50}Zr_{50}$-gettered high-purity (5N) Ar atmosphere. When melted under microgravity, the samples became perfectly spherical. The first two samples were transported to the ISS in metallic cage holders and the last one in a ceramic cup holder. The lower vapor pressure of the $Ti_{39.5}Zr_{39.5}Ni_{21}$, $Zr_{57}Cu_{15.4}Ni_{12.6}Al_{10}Nb_5$ liquids allowed the samples to be studied in the cage holder; the cup was used for the $Cu_{50}Zr_{50}$ to contain evaporation from this higher vapor pressure liquid. The ISS-EML facility[20,26,39] consists of two precisely aligned, identical water-cooled Cu coils. Two separate circuits feed rf voltages to these coils; one for positioning the sample at 150 kHz and the other for heating at 350 kHz. The currents in the two coils for the positioning field were supplied in the opposite directions to produce a quadrupole field. Since the samples were under microgravity, no levitating force was required; a small quadrupolar electromagnetic field provided enough force to keep the sample in position, which caused very limited heating of the sample. Heating currents circulated in the same direction so that a dipole rf electromagnetic field was produced. Unlike most ground-based EML facilities, the heating and positioning can therefore be controlled independently. Processing under high vacuum (~10^{-8} mbar) as well as in high-purity Ar- and He-gas atmospheres are possible.

Typically, the samples were heated 300−400 K above T_l and then allowed to cool under various combinations of positioner and heater voltages to induce various levels of stirring/fluid flows. The samples were monitored by two video cameras positioned along the polar and radial directions. The temperatures were measured by an optical pyrometer (1.45−1.80 μm) between 573 and 2373 K. Nucleation and subsequent growth of crystals were marked by a sudden rise in temperature, called recalescence, due to the release of latent heat of fusion. The nucleation temperatures were measured during several melting and solidification cycles under different fluid flow conditions. The measured temperatures were based on emissivity values and electromagnetic coupling coefficients of the samples with the heater and positioner coils, determined from ground-based studies. In actual experiments on the ISS, the sample position shifted, depending on the heater and positioner voltages applied. This changed the measured temperatures, which had to be corrected. This was performed using the measured liquidus temperatures on the ISS-EML and those measured by the DTA technique on ground using a relationship, $1/T_{correct} = 1//T_{measured} + 1/T_{correct\ liquidus} - 1/T_{measured\ liquidus}$, where all temperatures are in K. The experiments on each sample were conducted over several nights. The samples were stored in Helium gas during the intervening periods. In some cases, the nucleation temperatures increased during the initial thermal cycles compared to the previous night's operations. After a few melting cycles it reverted back to the previous values. Therefore, those initial cycles were excluded from the analysis. It was also observed that if the liquid was disturbed during cooling by pulsing for the viscosity measurements or the positioner/heater voltages were changed during cooling, the nucleation temperature changed. For those

reasons, the nucleation data from those cycles were also excluded. The reason for such changes is not clear at the moment. Maximum supercooling for the $Ti_{39.5}Zr_{39.5}Ni_{21}$ liquid was achieved after many melting cycles under vacuum over several nights. Possibly, the liquid purified during such repeated melting. The data presented here are from these later melting cycles when consistent maximum supercooling could be achieved.

Model calculations for fluid flow
Fluid flow velocities and shear rates are the two parameters that give a direct measure of the stirring. Since they cannot be measured directly in the present experimental arrangement, model calculations were necessary. The voltages and currents applied to the positioner and heater coils, their frequencies, the position and diameter of the sample with respect to the coils, sample electrical resistivity and coupling coefficient to the rf fields, the liquid viscosity and density as a function of temperature are the input parameters in this model[37,38]. The particular details of the coil geometry and the rf fields can be found elsewhere[39]. The temperature dependent viscosities of the liquids were measured by a ground-based ESL facility[40,41] at Washington University in St. Louis and were reported earlier[42,43]. A commercial software, ANSYS, was used to solve the Navier–Stokes equation under the conditions of the experiment. The model used was verified from an earlier experiment on the ISS where the flow rates were measured from video images of particles flowing on the surface of an immiscible CuCo liquid[44]; the model calculations agreed with the experimental results within 7%. Since the flows are laminar under the experimental conditions, a laminar flow model was used here.

Reporting summary
Further information on research design is available in the Nature Research Reporting Summary linked to this article.

DATA AVAILABILITY
The experimental data are available from the corresponding author on reasonable request.

CODE AVAILABILITY
A commercial software, ANSYS, was used to solve the Navier–Stokes equation to estimate the fluid flow velocities and shear rates.

REFERENCES
1. Kelton, K. F. & Greer, A. L. *Nucleation in Condensed Matter* (Elsevier, 2011).
2. Glicksman, M. E *Principles of Solidification* (Springer: 2011).
3. Herlach, D. M., Galenko, P. & Holland-Moritz, D. *Metastable Solids from Under-cooled Melts* (ed. Cahn, R. W.) (Elsevier, Amsterdam, 2007).
4. Rhim, W.-K., Collender, M., Hyson, M. T., Simms, W. T. & Elleman, D. D. Development of an electrostatic positioner for space material processing. *Rev. Sci. Instrum.* **56**, 307 (1985).
5. Herlach, D. M., Cochrane, R. F., Egry, I., Fecht, H.-J. & Greer, A. L. Containerless processing in the study of metallic melts and their solidification. *Int. Mat. Rev.* **38**, 273 (1993).
6. Weber, J. K. R. et al. Aeroacoustic levitation: a method for containerless liquid phase processing at high temperatures. *Rev. Sci. Instrum.* **65**, 456 (1994).
7. Trinh, E. H. Compact acoustic levitation device for studies in fluid dynamics and materials science in the laboratory and microgravity. *Rev. Sci. Instrum.* **56**, 2059 (1985).
8. Wedekind, J., Hyva ̈rinen, A.-P., Brus, D. & Reguera, D. Unraveling the pressure effect on nucleation. *Phys. Rev. Lett.* **101**, 125703 (2008).
9. Karpov, I. V. et al. Evidence of field induced nucleation in shape memory. *J. Appl. Phys.* **92**, 173501 (2008).
10. Hou, H. & Chang, H.-C. AC field enhanced protein crystallization. *Appl. Phys. Lett.* **92**, 223902 (2008).
11. Gavira, J. A. & Garcia-Ruiz, J. M. Effects of a magnetic field on Lysozyme crystal nucleation and growth in a diffusive environment. *Cryst. Growth Des.* **9**, 2610 (2009).

12. Schenk, T., Holland-Moritz, D. & Herlach, D. M. Observation of magnetically induced crystallization of undercooled Co-Pd alloys. *Europhys. Lett.* **50**, 402 (2000).

13. Holland-Moritz, D. & Spaepen, F. The magnetic contribution to the driving force for crystal nucleation in undercooled Co-Pd melts. *Philos. Mag.* **84**, 957 (2004).

14. Galenko, P. K., Reuther, K., Kazak, O. V., Alexandrov, D. V. & Rettenmayr, M. Effect of convective transport on dendritic crystal growth from pure and alloy melts. *Appl. Phys. Lett.* **111**, 031602 (2017).

15. Galenko, P. K. et al. Bell-shaped "dendrite velocity-undercooling" relationship with an abrupt drop of solidification kinetics in glass forming Cu-Zr(-Ni) melts. *J. Cryst. Growth* **532**, 125411 (2020).

16. Kelton, K. F. Time-dependent nucleation in partitioning transformations. *Acta Mater.* **48**, 1967 (2000).

17. Diao, J., Salazar, R., Kelton, K. F. & Gelb, L. D. Impact of diffusion on concentration profiles around near-critical nuclei and implications for theories of nucleation and growth. *Acta Mater.* **56**, 2585 (2008).

18. Wei, P. F., Kelton, K. F. & Falster, R. Coupled-flux nucleation modeling of oxygen precipitation in silicon. *J. Appl. Phys.* **88**, 5062 (2000).

19. Getting, A. V. *Rayleigh-Benard Convection: Structures and Dynamics* (World Scientific, 1988).

20. Seidel, A., Soellner, W. & Stenzel, C. EML—an electromagnetic levitator for the International Space Station. *J. Phys. Conf. Ser.* **327**, 012057 (2011).

21. Kelton, K. F. et al. First X-ray scattering studies on electrostatically levitated metallic liquids: demonstrated influence of local icosahedral order on the nucleation barrier. *Phys. Rev. Lett.* **90**, 195504 (2003).

22. Lee, G. W., Croat, T. K., Gangopadhyay, A. K. & Kelton, K. F. Icosahedral-phase formation in as-cast Ti-Zr-Ni alloys. *Philos. Mag. Lett.* **82**, 199 (2002).

23. Gegner, J. et al. In situ observation of the phase selection from the undercooled melt in Cu-Zr. *J. Alloy. Comp.* **576**, 232 (2013).

24. Okamoto, H. Cu-Zr phase diagram. *J. Phase Equilibria Diffus.* **29**, 204 (2008).

25. Shadowspeaker, L., Shah, M. & Busch, R. On the crystalline equilibrium phases of the $Zr_{57}Cu_{15.4}Ni_{12.6}Al_{10}Nb_5$ bulk metallic glass forming alloy. *Scr. Metal.* **50**, 1035 (2004).

26. Lohoefer, G. High-resolution inductive measurement of electrical resistivity and density of electromagnetically levitated liquid metal droplets. *Rev. Sci. Instrum.* **89**, 124709 (2018).

27. Bendert, J. C., Blodgett, M. E., Gangopadhyay, A. K. & Kelton, K. F. Measurements of volume, thermal expansion, and specific heat in $Zr_{57}Cu_{15.4}Ni_{12.6}Al_{10}Nb_5$ and $Zr_{58.5}Cu_{15.6}Ni_{12.8}Al_{10.3}Nb_{2.8}$ liquids and glasses. *Appl. Phys. Lett.* **102**, 211913 (2013).

28. Mohr, M., Wunderlich, R. K., Hofmann, D. C. & Fecht, H.-J. Thermophysical properties of liquid $Zr_{52.5}Cu_{17.9}Ni_{14.6}Al_{10}Ti_5$—prospects for bulk metallic glass manufacturing in space. *npj Microgravity* **5**, 24 (2019).

29. Sellers, M. E. *Studies of Maximum Supercooling and Stirring in Levitated Liquid Metal Alloys*. Ph.D. Thesis, Washington University in St. Louis (2020).

30. Schenk, T., Holland-Moritz, D., Simonet, V., Bellisent, R. & Herlach, D. M. Icosahedral short range order in deeply undercooled metallic melts. *Phys. Rev. Lett.* **89**, 075507 (2002).

31. Lee, G. W., Gangopadhyay, A. K. & Kelton, K. F. Phase diagram studies of Ti-Zr-Ni alloys containing less than 40 at.% Ni and estimated critical cooling rate for icosahedral quasicrystal formation from the liquid. *Acta Mater.* **59**, 4964 (2011).

32. Sellers, M. E., Van Hoesen, D. C., Gangopadhyay, A. K. & Kelton, K. F. Maximum supercooling studies in $Ti_{39.5}Zr_{39.5}Ni_{21}$, $Ti_{40}Zr_{30}Ni_{30}$, $Zr_{80}Pt_{20}$—connecting liquid structure and the nucleation barrier. *J. Chem. Phys.* **150**, 204510 (2019).

33. Skripov, V. P. Homogeneous nucleation in melts and amorphous films. in *Crystal Growth and Materials* (Current Topics in Materials Science), Vol. 2 (eds. Kaldis, E. and Scheel, H. J.) 328–378 (North-Holland, 1977).

34. Morton, C. W., Hofmeister, W. H., Bayuzick, R. J., Rulison, A. J. & Watkins, J. L. The kinetics of solid nucleation in Zirconium. *Acta Mater.* **46**, 6033 (1998).

35. Klein, S., Holland-Moritz, D. & Herlach, D. M. Crystal nucleation in undercooled liquid zirconium. *Phys. Rev. B* **80**, 212202 (2009).

36. Turnbull, D. Formation of crystal nuclei in liquid metals. *J. Appl. Phys.* **21**, 1022 (1950).

37. Hyers, R. W., Matson, D. M., Kelton, K. F. & Rogers, J. R. Convection in containerless processing. *Ann. N. Y. Acad. Sci.* **1027**, 474 (2004).

38. Bracker, G. P. et al. The effect of flow regimes on the surface oscillations during electromagnetic levitation experiments. *High. Press. High. Temp.* **49**, 49 (2020).

39. Lohöfer, G. & Piller, J. The new ISS electromagnetic levitation facility—'MSLEML'. in *40th AIAA Aerospace Sciences Meeting & Exhibit* (American Institute of Aeronautics and Astronautics, 2002).

40. Gangopadhyay, A. K. et al. Beamline electrostatic levitator for in-situ high energy x-ray diffraction studies of levitated solids and liquids. *Rev. Sci. Instrum.* **76**, 073901 (2005).

41. Mauro, N. A. & Kelton, K. F. A highly modular beamline electrostatic levitation facility, optimized for in situ high-energy x-ray scattering studies of equilibrium and supercooled liquids. *Rev. Sci. Instrum.* **82**, 035114 (2011).

42. Bradshaw, R. C. et al. Nonlinearities in the undercooled properties of $Ti_{39.5}Zr_{39.5}Ni_{21}$. *Philos. Mag.* **86**, 341 (2006).

43. Blodgett, M. E., Egami, T., Nussinov, Z. & Kelton, K. F. Proposal for universality in the viscosity of metallic liquids. *Sci. Rep.* **5**, 13837 (2015).

44. Lee, J. et al. Magnetohydrodynamic modeling and experimental validation of convection inside electromagnetically levitated Co-Cu droplets. *Metall. Mater. Trans. B* **45**, 1018 (2014).

ACKNOWLEDGEMENTS

AUTHOR CONTRIBUTIONS

K.F.K. conceived the idea. A.K.G., D.H.-M., S.K., P.K.G., and K.F.K. planned the experiments. A.K.G. and S.K. prepared the samples. A.K.G., D.H.-M., D.C.V.H. and K.F.K. performed the experiments in cooperation with the members of the Microgravity Users Support Center at the DLR, Köln. A.K.G., M.E.S. and D.H.-M. analyzed the data. G. P.B., A.K.P. and R.W.H. performed the fluid flow calculations. A.K.G. and K.F.K wrote the manuscript with inputs from all coauthors.

COMPETING INTERESTS

The authors declare no competing interests.

ADDITIONAL INFORMATION

Supplementary information The online version contains supplementary material available at https://doi.org/10.1038/s41526-021-00161-9.

Correspondence and requests for materials should be addressed to A.K.G.

Reprints and permission information is available at http://www.nature.com/reprints

Publisher's note Springer Nature remains neutral with regard to jurisdictional claims in published maps and institutional affiliations.